Blowup dynamics of coherently driven polariton condensates: Experiment

S. S. Gavrilov,[1] A. S. Brichkin,[1] Ya. V. Grishina,[1,2] C. Schneider,[3] S. Höfling,[3] and V. D. Kulakovskii[1]
[1]*Institute of Solid State Physics, RAS, Chernogolovka 142432, Russia*
[2]*Faculty of Fundamental Physical and Chemical Engineering, M. V. Lomonosov Moscow State University, Moscow 119991, Russia*
[3]*Technische Physik, Physikalisches Institut and Wilhelm Conrad Röntgen Research Center for Complex Material Systems, Universität Würzburg, D-97074 Würzburg, Germany*
(Received 30 July 2015; revised manuscript received 6 November 2015; published 30 November 2015)

We report an experimental verification of the recent prediction that sharp transitions between steady states in multistable cavity-polariton systems are mediated by intermode parametric scattering that triggers the accumulation of energy and, hence, lowers the threshold at the cost of extending the transition latency period [S. S. Gavrilov, Phys. Rev. B **90**, 205303 (2014)]. The time-resolved measurements are performed using a high-Q GaAs microcavity pumped slightly above the lower polariton level at normal incidence.

DOI: 10.1103/PhysRevB.92.205312 PACS number(s): 71.36.+c, 42.65.Pc, 42.50.Pq

I. INTRODUCTION

Optical multistability in cavity-polariton systems attracts much attention as it enables one to implement controllable ultrafast all-optical switches of microcavities on the time scale of several picoseconds [1–11]. Cavity polaritons are composite bosons formed by strongly coupled excitons and cavity photons [12]. Polaritons form a macroscopically coherent state under resonant and coherent optical driving. Due to the exciton component, they feature mutual repulsion that involves a considerable blueshift of their resonance energy with increasing density. As a result, the system of cavity polaritons can be considered as a nonequilibrium Bose condensate and described using the Gross-Pitaevskii equations, similar to condensates of cold atoms and, generally speaking, to macroscopically coherent states in superconductors, yet both the finite lifetime of polaritons and external driving should be explicitly taken into account [13].

Polariton multistability occurs when the pump frequency ω_p exceeds the polariton level ω [1,2,14–20]. Its physical origin stems from the positive feedback loop between the amplitude and effective resonance frequency, so that on reaching the threshold, the field grows until pump detuning $D = \omega_p - \omega > 0$ gets virtually compensated due to the resonance-shift effect. Such a system bears two steady-state branches under a circularly polarized pump when only one of the two polariton spin components is excited. This is the case discussed in our current study; note, however, that in a general case, polariton condensates can exhibit a richer multistable behavior due to the spin anisotropy of the polariton-polariton interaction [3,21].

The one-mode "bistable" dependence of the cavity-field intensity $|\psi|^2$ on pump intensity has the form of an S-shaped curve. In general, the one-mode approximation can be inappropriate to describe system dynamics; in such cases, the many-mode Gross-Pitaevskii equations were solved numerically in a number of works. Nevertheless, it was usually accepted that under plane-wave excitation at normal incidence, the threshold for the transition to the upper state corresponds to the right turning point of the S-shaped curve where its lower steady-state branch terminates [1–8,15]. Provided the polariton decay rate γ is much smaller than D, the critical cavity-field intensity in the turning point amounts to $|\psi|^2 \approx D/3V$, where V is the polariton-polariton interaction constant [2]. However, recently it was theoretically found that the transition to the upper one-mode state must start upon reaching the parametric scattering threshold $|\psi|^2 \approx \gamma/V$, even at $\gamma \ll D$ [20]. Instead of an immediate jump into the high-field state, under constant pumping the field is gradually accumulated in scattered modes and, only when it becomes sufficiently strong, it induces a sharp jump in the driven mode. Thus, the transition has a latency period between reaching the threshold intensity and the sharp jump in the cavity field. Its duration can largely exceed the polariton lifetime in a case when $\gamma \ll D$ and the pump power is comparatively weak. This effect was not previously considered in polariton physics, even in the context of essentially many-mode Gross-Pitaevskii equations. Similar scenarios that imply a hyperbolic growth, so that under fixed external conditions an arbitrarily "slow" dynamics ends up with an explosive amplification, are known as regimes "with blowup" [22].

This study is devoted to an experimental verification of the blowup dynamics in bistable polariton condensates under coherent optical driving. The evolution is studied with momentum-space and time resolutions under 200-ps-long pump pulses acting at normal incidence. In our system, $Q \gtrsim 10^4$ and $D/\gamma \gtrsim 10$. We have found that near the threshold, the sharp jump in the cavity-field intensity is delayed by about 50 ps with respect to the pulse maximum. No such delay is observed in the linear regime in which the time shape of the field transmitted through the cavity merely reproduces external driving. Above the threshold, scattered modes with different momenta are found to spring up within the time interval between reaching the threshold and the jump in the cavity field. The experimental results are reproduced numerically using the Gross-Pitaevskii equations. We deduce that our observations reveal an energy accumulation process and confirm the conclusions of Ref. [20].

The paper is organized as follows. In Sec. II, we summarize the theoretical predictions and demonstrate them numerically with 200 ps pump pulses. In Sec. III A, the sample and experimental setup are described, and in Sec. III B, we compare the experimental and theoretical data. Section IV contains concluding remarks.

II. THEORETICAL AND NUMERICAL EXPECTATIONS

According to Ref. [20], transitions between steady states in a bistable polariton system are mediated by intermode parametric scattering. In high-Q cavities, the scattering threshold $V|\psi|^2 = \gamma$ can be much smaller than that of a "one-mode bistable transition." The scattered states are fed by the externally pumped mode that breaks up into various signal/idler pairs on reaching the threshold. This, however, does not prevent further growth of the pumped mode even under constant excitation conditions. The positive feedback loop between the pumped mode and scattered states leads to a gradual accumulation of energy and then to a sharp jump into the high-field state in which the polariton resonance is shifted up to the pump frequency, so that eventually $V|\psi|^2$ increases from $\sim\gamma$ to $\sim D$. Formally, the amplification factor D/γ can be arbitrarily large, yet the jump is then markedly delayed in time with respect to the moment of reaching the threshold density. Such a delay is the cost paid for the drastic lowering of the threshold pump power compared to the threshold for the strictly one-mode condensate that is incapable of a "slow" energy accumulation.

The above scenario is found [20] to be a general property of dynamical systems governed by the Gross-Pitaevskii equation,

$$i\frac{\partial\psi}{\partial t} = [\omega(-i\nabla) - i\gamma + V|\psi|^2]\psi + f(t). \tag{1}$$

Here both the condensate amplitude (ψ) and driving field (f) are complex-valued functions of time and coordinates within the two-dimensional active cavity layer. $|f|^2$ has the meaning of the pump intensity. Function $\omega = \omega(-i\nabla)$ corresponds to the dispersion law for the low-polariton branch, which in the momentum space reads

$$\omega(k) = \frac{\omega_C(k) + \omega_X}{2} - \frac{1}{2}\sqrt{[\omega_C(k) - \omega_X]^2 - R^2}, \tag{2}$$

where k is the in-plane wave number, $\omega_{X,C}$ are the frequencies of the exciton and the cavity photon, respectively, and R is the Rabi splitting. In its turn,

$$\omega_C(k) = \omega_C(0) + \frac{\hbar k^2}{2m_C}, \quad m_C = \frac{\epsilon\hbar\omega_C(0)}{c^2}. \tag{3}$$

Exciton effective mass m_X is much larger than m_C, so the k-space dependence of ω_X can be neglected at small k. We also neglect the k dependences of γ and V on the assumption that the pump acts far below the exciton level and $[\omega_p - \omega(k=0)] \ll \omega_X - \omega_p$.

The one-mode stationary response function ($|\psi|^2$ vs space- and time-independent $|f|^2$) has the form of an S-shaped curve [1,2] (Fig. 1). Under pumping at $k = 0$ and positive frequency mismatch $D = \omega_p - \omega(k=0) > \gamma$, the parametric scattering threshold reads

$$F_P^2 = \frac{\gamma}{V}[(D-\gamma)^2 + \gamma^2]. \tag{4}$$

That is the value of pump intensity $|f|^2$ at which the driven polariton mode ($k = 0$) starts breaking up into "signals" (s) and "idlers" (i) obeying phase-matching conditions $\mathbf{k}_i = -\mathbf{k}_s$ and $\omega_s = \omega_i = \omega_p$ [20,23,24]. On the other hand, the one-mode

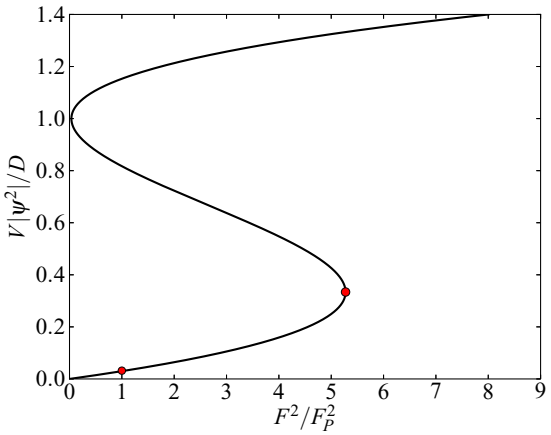

FIG. 1. (Color online) One-mode solutions of Eq. (1) with $f(\mathbf{k},t) = F\delta(\mathbf{k})e^{-i\omega_p t}$, depending on F^2. Circles indicate the scattering threshold [$F = F_P$, Eq. (4)] and bistability turning point [$F = F_B$, Eq. (5)]. The solutions are obtained at $\hbar\gamma = 0.028$ meV and $\hbar D = 0.9$ meV.

bistability turning point is [2]

$$F_B^2 = \frac{2}{27V}[D^3 + 9D\gamma^2 + (D^2 - 3\gamma^2)^{3/2}]. \tag{5}$$

The bistability *per se* exists so long as $D > \sqrt{3}\gamma$; the middle branch with a negative slope is asymptotically unstable.

Renormalization of the polariton dispersion law with increasing $|\psi|$ is illustrated in Fig. 2. The signal and idler eigenfrequencies read [1,13–15,20]

$$\tilde{\omega}(k) = \omega_p - i\gamma \pm \sqrt{[\omega_p - \omega(k) - 2V|\psi^2|]^2 - (V|\psi^2|)^2}. \tag{6}$$

They tend to the bare dispersion law $\omega(k)$ (2) and its idler counterpart $2\omega_p - \omega(-k)$ at $\psi \to 0$ [Fig. 2(a)]. The scattering signal positions k_s are given by their intersections at $\omega = \omega_p$. Decay rates $\mathrm{Im}\,\tilde{\omega}(k_s)$ turn to zero for a certain k_s in the threshold point $V|\psi|^2 = \gamma$ and, accordingly, the k dependence of $\mathrm{Re}\,\tilde{\omega}$ acquires a flat region near k_s. With further increasing

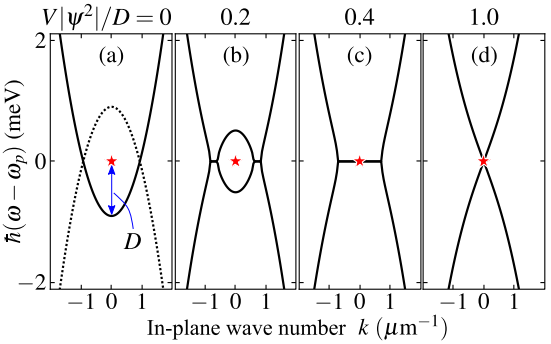

FIG. 2. (Color online) (a) Unperturbed polariton dispersion $\omega(k)$ (solid line) and its "idler" counterpart $2\omega_p - \omega(-k)$ (dotted line). Frequencies are reckoned from the pump mode. (b)–(d) Renormalized "signal" and "idler" dispersion branches at $V|\psi^2|/D = 0.2$, 0.4, and 1.0, respectively. Stars indicate the pump position. Intersections of signal and idler branches within flat regions in (b) and (c) comprise unstable modes. The parameters agree with those in Fig. 1.

$|\psi|$, the instability region extends in the k space towards $k = 0$ [Fig. 2(b)]. The range of $|\psi|$ in which the $k = 0$ mode falls within the instability region [as in Fig. 2(c)] corresponds to the solutions with a negative slope in Fig. 1. Finally, Fig. 2(d) makes it clear that the intermode scattering can no longer occur on the upper branch of the S curve. Thus, bistability and parametric scattering stem from the common physical origin and are closely related to each other.

To compare the solutions of Eq. (1) with the experiment, we chose a pump source taking the form

$$f(\mathbf{k},t) = F\frac{e^{-\mathbf{k}^2/2\sigma_K^2}}{\cosh(-t/\tau)}e^{-i\omega_p t} + a\xi(\mathbf{k},t), \qquad (7)$$

where τ and σ_K^{-1} determine the pulse duration and the size of the pump spot, respectively. The second term, $\xi(\mathbf{k},t)$, represents a stochastic Langevin force that is a white noise, i. e., $\langle\xi(\mathbf{k},t)\rangle = 0$ and $\langle\xi(\mathbf{k},t)\xi(\mathbf{k}',t')\rangle = \delta(\mathbf{k}-\mathbf{k}')\delta(t-t')$. Equation (1) is solved on a 81×81 grid in the k space with $-2.5 \leqslant k_{x,y} \leqslant 2.5\ \mu\mathrm{m}^{-1}$. The noise phases $\arg\xi(\mathbf{k},t)$ change randomly each 50 fs at each grid node $\mathbf{k}$. The noise amplitude a is such that the noise term alone would provide a weak steady-state population $V|\psi|^2 \lesssim 10^{-5}\gamma$ for each $\mathbf{k}$.

The chosen parameters are dielectric constant $\epsilon = 12.5$ (corresponds to GaAs), photon-exciton frequency mismatch $\hbar[\omega_C(0) - \omega_X] = -5$ meV, Rabi splitting $\hbar R = 10.5$ meV, low-polariton decay rate $\hbar\gamma = 0.028$ meV, and pump frequency detuning $\hbar D \equiv \hbar[\omega_p - \omega(k=0)] = 0.9$ meV. The units for ψ and f are fixed by condition $V = 1$, so that $|\psi|^2$ has the dimension of frequency and the meaning of resonance blueshift.

Consider the evolution of the polariton condensate under pulsed excitation with finite τ and only one macro-occupied spatial harmonic ($\sigma_K = 0$). Such a system exhibits fast jumps in $|\psi|$ when F^2 exceeds turning point (5). Decreasing F involves extension of the latency period that becomes infinitely long at $F \to F_P$. Thus, the shorter is pulse duration τ, the larger is the effective threshold pump intensity $W_{\mathrm{thr}} \equiv F_{\mathrm{thr}}^2$ at which a jump in $|\psi|$ gets observable within the pulse. Our calculations show that at $\tau = 100$ ps and $\sigma_K = 0$ and the chosen noise parameters, the threshold amounts to $F_{\mathrm{thr}}^2 \approx 2.5F_P^2$, which is approximately twice smaller than $F_B^2 \approx 5F_P^2$.

Figure 3 shows the dynamics of the driven mode ($k = 0$) and scattered modes at $\tau = 100$ ps and different peak pump intensities $W \equiv F^2$. The driven mode intensity $I_0(t) = |\psi(k=0,t)|^2$ is divided by W, so its time dependences repeat each other in the linear regime (at $t \lesssim 50$ ps) [Fig. 3(a)]. Figure 3(b) shows the ratio between $I_S(t) = \sum_{\mathbf{k}}|\psi(\mathbf{k},t)|^2$ at $0.4 < |\mathbf{k}| < 1.7\ \mu\mathrm{m}^{-1}$ and $I_0(t)$. This ratio reflects the effect of the intermode parametric scattering. Note that at $|f| = F_P$, the scattering signals are located at $|\mathbf{k}| \approx 1\ \mu\mathrm{m}^{-1}$, in accordance with the dispersion law.

At $W = 0.3W_{\mathrm{thr}}$, the system is in the linear regime, so that $I_0(t)$ merely reproduces the pump shape. Immediately above parametric scattering threshold F_P, the signals still cannot get strong enough to provide a visible feedback to the driven mode within the pulse. By contrast, at $W = W_{\mathrm{thr}} \approx 2.5F_P^2 \approx 0.5F_B^2$, the integral signal intensity reaches a "macroscopic" level by $t = 0$ and, at the same time, the driven mode shows a superlinear growth with increasing $|f(t)|$. Thus, there is a

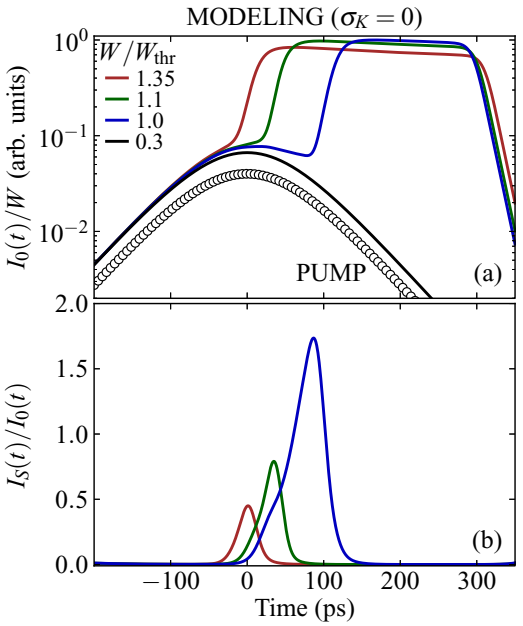

FIG. 3. (Color online) Solutions of Eq. (1) under pumping (7) with $\tau = 100$ ps, $\sigma_K = 0$, and different peak intensities $W \equiv F^2$. (a) Intensities of the driven mode $I_0(t) = |\psi(k=0,t)|^2$ divided by W. The pump shape is shown by the thick line. (b) Ratios between total intensity I_S of scattered modes at $0.4 < |\mathbf{k}| < 1.7\ \mu\mathrm{m}^{-1}$ and $I_0(t)$.

positive feedback loop between the driven mode and the set of scattered modes. Immediately after $t = 0$, they grow much more rapidly compared to the decrease of the pump intensity. By $t \approx 90$ ps, the system reaches the "blowup point" [20] in which the upper steady state becomes the only attractor, and I_0 grows explosively. The polariton resonance is blueshifted up to the pump frequency, so scattering becomes no longer possible in accordance with the phase-matching conditions. Thereafter, the signals at $k \neq 0$ reduce down to the noise level and the system resides in the upper one-mode state until the pump falls below the backward turning point of the S curve, $|f|^2 \approx 2\gamma^2 D/27V$, where the system experiences backward transition ($t \approx 300$ ps).

Both the blowup time and ratio I_S/I_0 decrease with increasing W. Eventually, at $F^2 > F_B^2$, no scattered states are needed for the transition to happen.

In the following section, we compare the theoretical estimates with the experiment. To this end, we have to take into consideration a finite size of the pump spot ($\sigma_K > 0$).

III. EXPERIMENT

A. Sample and setup

The microcavity sample is grown by molecular-beam epitaxy on top of a GaAs substrate. The cavity top and bottom mirrors consist of 32 and 36 $Al_{0.2}Ga_{0.8}As/AlAs$ Bragg reflectors, respectively. The Q factor exceeds 10^4. Four 7-nm-thick GaAs quantum wells separated by 4 nm AlAs barriers are within the $\lambda/2$ active layer, and eight other quantum wells are in the neighboring AlAs layers. The resulting Rabi splitting is 10.5 meV. The detuning between

the cavity and exciton modes $\hbar[\omega_C(0)-\omega_X]$ varies along the cavity plane from -8 meV to 0; at the studied location, it equals -5 meV. A 700×300 μm window is etched out of the GaAs substrate using citric acid/hydrogen peroxide selective etch in order to perform transmission measurements. The decay rate of the low-polariton states obtained from the time-resolved transmission measurements is $\gamma\sim0.02$ meV, while the inhomogeneously broadened spectra measured under 1 ps pulses reveal the full width at half maximum (FWHM) of about 0.12 meV near $k=0$.

The sample is placed into an optical cryostat at $T\sim10$ K. The cavity is excited slightly above the low-polariton resonance ($D\approx1$ meV) by circularly polarized optical pulses generated by a mode-locked Ti:sapphire laser with a repetition rate of 80 MHz and pulse duration of 200 ps. The laser beam is directed along the normal to the cavity plane and focused into a 45 μm (FWHM) spot on the sample. The optical pulses transmitted through the cavity are detected by a Synchro Scan streak camera with a time resolution of 3 ps and angle resolution of 1° in the x direction ($\Delta k_x\sim0.1$ μm^{-1}). In the y direction, the signal is integrated over 3° ($-0.2\lesssim k_y\lesssim0.2$ μm^{-1}).

The modeling parameters chosen in Sec. II match the considered system parameters.

B. Comparison to the theory

Figure 4(a) shows the time dependences of the transmission signal intensity I_0 at $|k_x|<0.1$ μm^{-1}, $|k_y|<0.2$ μm^{-1}, and different peak pump intensities W. The pulse shape is shown for reference in arbitrary units. The experimentally estimated threshold intensity is 4 kW/cm^2. The measured signal intensities $I_0(t)$ are divided by W, which makes them coincide in the linear regime and simplifies their comparison. The intensity ratios between the scattered modes (summed up over $0.4<|k_x|<1.7$ μm^{-1}, $|k_y|<0.2$ μm^{-1}) and $I_0(t)$ are shown in Fig. 4(c). For completeness, we also show raw streak camera images of the signal intensity distributions $I(k_x,t)$ at $-0.2<k_y<0.2$ μm^{-1} (Fig. 5).

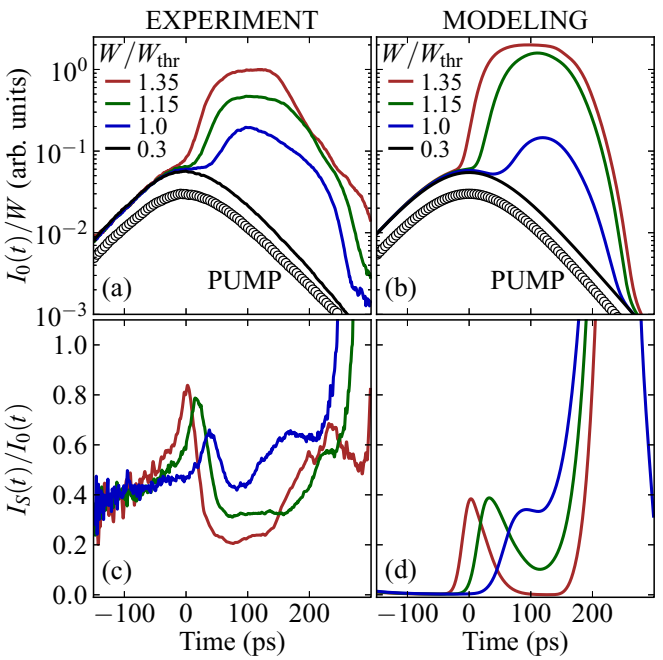

FIG. 4. (Color online) (a), (c) Measured and (b), (d) calculated dynamics of the polariton system under pumping with $\tau=100$ ps, $\sigma_K=0.037$ μm^{-1}, and different peak intensities W. (a), (b) Intensities $I_0(t)$ of the driven mode ($k=0$) divided by W. (c), (d) Ratios between the intensity of scattered modes at $0.4<|\mathbf{k}|<1.7$ μm^{-1} and $I_0(t)$. In the experiment, the signal was collected from a narrow strip in the k_y direction, $|k_y|<0.2$ μm^{-1}.

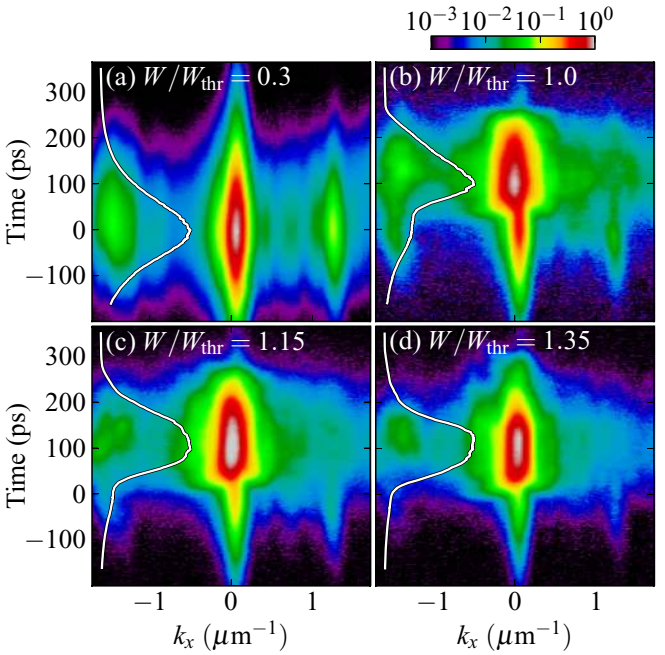

FIG. 5. (Color online) Streak camera images of the signal intensity distributions $I(k_x,t)$ summed up over k_y in the interval $-0.2<k_y<0.2$ μm^{-1} at different W. Each image is normalized to 1 and covers four orders of magnitude in a logarithmic scale. Lines represent the time dependences of $I_0=|\psi(k=0)|^2$ in an arbitrary linear scale.

The modeled counterparts of Figs. 4(a) and 4(c) are presented in Figs. 4(b) and 4(d). Unlike Fig. 3, they are (i) calculated with a finite pump spot size ($\sigma_K=0.037$ μm^{-1}, the FWHM of $|f|^2$ being 45 μm) and (ii) averaged over a large series with partially random peak intensities that obey a Gaussian distribution with a standard deviation of $0.05\,W$ for each W. Under such conditions, the effective threshold is $W_{\rm thr}\approx3F_P^2$.

From Fig. 4(a), it is seen that below the threshold ($W=0.3W_{\rm thr}$), the signal nearly repeats the pulse shape. Thus, the system has no intrinsic "inertness" with respect to external driving. This is fairly natural as the substrate layer was removed and the thickness of the pumped area does not exceed ~100 μm. At the same time, the pump acts far below the free exciton level [$\hbar(\omega_p-\omega_X)\approx-8.3$ meV], which ensures excitation of only the short-lived polariton states rather than the long-lived excitons that in other circumstances could accumulate and thus yield a reservoir effect [7,25,26]. The corresponding k-space distribution at $W=0.3W_{\rm thr}$ [Fig. 5(a)] reveals a Rayleigh scattering signal

at $\omega \approx \omega_p$, $|k_x| \approx 1.3\ \mu\text{m}^{-1}$. The signal is a bit asymmetric due to an inevitable potential disorder.

At the threshold ($W = W_{\text{thr}}$), the transmission signal springs up with a marked delay with respect to the peak of the excitation. [Fig. 4(a)]. The jump is preceded by the rise of scattered modes [Fig. 4(c)]. The sharp increase in I_S/I_0 evidences the thresholdlike polariton-polariton scattering as opposed to thresholdless Rayleigh scattering or ballistic expansion. The k-space distribution [Fig. 5(b)] gets flattened in the vicinity of $k = 0$ immediately before the jump in the $k = 0$ mode intensity. This can be associated with the many-mode instability: The signal and idler dispersion surfaces stick together at $\omega_s = \omega_i = \omega_p$ within a flat area centered at $k = 0$, so that various scattering processes of the type $(0,0) \rightarrow (\mathbf{k}, -\mathbf{k})$ become simultaneously allowed by the phase-matching conditions. Such a state is strongly unstable and, according to Ref. [20], it must result in a catastrophic amplification (rather than decay) of the $k = 0$ mode, which indeed occurs in the experiment.

With further increasing W, the blowup time decreases and the system is able to actually reach a high-field state in which D is nearly compensated due to the blueshift, at least in the spot center. This is evidenced by a plateau seen in the time dependence of I_0 in Fig. 4(a) and by a marked decrease in I_S/I_0 [Fig. 4(b)].

The numerical simulations presented in Figs. 4(b) and 4(d) reproduce all of the main features of the discussed process. Note, however, the differences between the cases of plane-wave ($\sigma_K = 0$, Fig. 3) and spatially limited excitation. First, it is seen that at $\sigma_K = 0$, all of the high-field states share nearly the same intensity I_0 determined by D. By contrast, under a Gaussian-shaped pumping, the area of the high-field states widens in the real space [4] with increasing W and, consequently, the peak amplitude of the $k = 0$ mode also increases. In fact, both the forward and backward transitions are spread in space and time due to the inhomogeneity of the excitation. For instance, the high-field area narrows down after $t \sim 100$ ps; therefore, I_0 decreases smoothly instead of a sharp drop as that seen in Fig. 3(a). On the other side, when the jump finishes in the spot center, there still exist the outer and thus weakly pumped areas that experience intermode scattering. Therefore, at $\sigma_K > 0$, the scattering into $k \neq 0$ does not terminate above threshold and the high-field state of a system as a whole is not truly one mode [Figs. 5(b)–5(d)].

Thus, we observe a good agreement between the theory and the experiment in which the transitions between steady states are studied with time resolution. All of the essential "control parameters" of Fig. 4(a)—amplification magnitudes and durations, latency periods, and dynamics as a whole for several pump powers—are reproduced and explained self-consistently. The polariton potential disorder was not taken into account in the simulations and, as a result, no "background" filling ($I_S/I_0 \approx 0.4$) related to Rayleigh scattering was reproduced numerically. Note, however, that potential fluctuations and/or spatially dependent states do not play any distinctive role in the studied phenomenon. Inhomogeneities only hamper the discussed evolution scenario. They can make the transition spread in time [11], but cannot make the transition starting point be delayed with respect to the pulse maximum. Such a delay, together with the sharp rise of scattered modes before the jump in the $k = 0$ mode intensity, constitute clear evidence of the energy accumulation process considered in Ref. [20].

IV. CONCLUSION

In this work, we have found that the intermode parametric scattering in a bistable polariton condensate facilitates the transition to the upper steady-state branch and thus lowers the threshold at the cost of transition-delay time.

Together with the theoretical work [20], our current study reveals the interrelation between the multistability and parametric scattering in resonantly driven cavity-polariton systems. Under slightly above-resonance pumping near normal incidence, the rise of the scattering cannot be considered as a second-order phase transition in spite of the "soft" type of the instability at the threshold point. Although the increase of scattered modes can be slow immediately on reaching the threshold, it successively involves (i) a positive feedback loop between the driven mode and scattered signals; (ii) a many-mode catastrophe when a multitude of scattered states is amplified concurrently, resulting in (iii) a sharp jump in the driven mode.

Under sufficiently long-term excitation, the threshold value of $V|\psi^2|$ is expected to reduce down to γ, while in the upper steady state, $V|\psi^2|$ exceeds pump detuning D [20]. Thus, formally, the cavity-field amplification factor D/γ becomes arbitrarily large with either increasing D or decreasing γ. It is not surprising that decreasing the decay rate makes a conventional (even linear) oscillator accumulate larger energy, provided the pump is not detuned from resonance. On the other hand, the fact that the pump frequency detuning is converted into the increased field ($\Delta|\psi^2| \sim D/V$) is a unique property of polariton condensates and other systems governed by Eq. (1). It may find use in the new-generation fast optical switches and logic elements.

ACKNOWLEDGMENTS

We are grateful to N. A. Gippius and S. G. Tikhodeev for fruitful discussions and to A. V. Sekretenko and A. V. Larionov for the assistance with the experiment. The visualizations are performed using MATPLOTLIB [27]. The work was supported by the Russian Science Foundation (Grant No. 14-12-01372).

[1] N. A. Gippius, S. G. Tikhodeev, V. D. Kulakovskii, D. N. Krizhanovskii, and A. I. Tartakovskii, Europhys. Lett. **67**, 997 (2004).

[2] A. Baas, J. P. Karr, H. Eleuch, and E. Giacobino, Phys. Rev. A **69**, 023809 (2004).

[3] N. A. Gippius, I. A. Shelykh, D. D. Solnyshkov, S. S. Gavrilov, Y. G. Rubo, A. V. Kavokin, S. G. Tikhodeev, and G. Malpuech, Phys. Rev. Lett. **98**, 236401 (2007).

[4] I. A. Shelykh, T. C. H. Liew, and A. V. Kavokin, Phys. Rev. Lett. **100**, 116401 (2008).

[5] D. N. Krizhanovskii, S. S. Gavrilov, A. P. D. Love, D. Sanvitto, N. A. Gippius, S. G. Tikhodeev, V. D. Kulakovskii, D. M. Whittaker, M. S. Skolnick, and J. S. Roberts, Phys. Rev. B **77**, 115336 (2008).
[6] T. K. Paraïso, M. Wouters, Y. Léger, F. Morier-Genoud, and B. Deveaud-Plédran, Nat. Mater. **9**, 655 (2010).
[7] D. Sarkar, S. S. Gavrilov, M. Sich, J. H. Quilter, R. A. Bradley, N. A. Gippius, K. Guda, V. D. Kulakovskii, M. S. Skolnick, and D. N. Krizhanovskii, Phys. Rev. Lett. **105**, 216402 (2010).
[8] C. Adrados, A. Amo, T. C. H. Liew, R. Hivet, R. Houdré, E. Giacobino, A. V. Kavokin, and A. Bramati, Phys. Rev. Lett. **105**, 216403 (2010).
[9] S. S. Gavrilov, A. V. Sekretenko, S. I. Novikov, C. Schneider, S. Höfling, M. Kamp, A. Forchel, and V. D. Kulakovskii, Appl. Phys. Lett. **102**, 011104 (2013).
[10] S. S. Gavrilov, A. V. Sekretenko, N. A. Gippius, C. Schneider, S. Höfling, M. Kamp, A. Forchel, and V. D. Kulakovskii, Phys. Rev. B **87**, 201303 (2013).
[11] A. V. Sekretenko, S. S. Gavrilov, S. I. Novikov, V. D. Kulakovskii, S. Höfling, C. Schneider, M. Kamp, and A. Forchel, Phys. Rev. B **88**, 205302 (2013).
[12] C. Weisbuch, M. Nishioka, A. Ishikawa, and Y. Arakawa, Phys. Rev. Lett. **69**, 3314 (1992).
[13] I. A. Shelykh, A. V. Kavokin, Y. G. Rubo, T. C. H. Liew, and G. Malpuech, Semicond. Sci. Technol. **25**, 013001 (2010).
[14] I. Carusotto and C. Ciuti, Phys. Rev. Lett. **93**, 166401 (2004).
[15] D. M. Whittaker, Phys. Rev. B **71**, 115301 (2005).
[16] S. S. Gavrilov, N. A. Gippius, V. D. Kulakovskii, and S. G. Tikhodeev, J. Expt. Theor. Phys. **104**, 715 (2007).
[17] M. Wouters and I. Carusotto, Phys. Rev. B **75**, 075332 (2007).
[18] S. S. Gavrilov, N. A. Gippius, S. G. Tikhodeev, and V. D. Kulakovskii, J. Expt. Theor. Phys. **110**, 825 (2010).
[19] S. S. Gavrilov and N. A. Gippius, Phys. Rev. B **86**, 085317 (2012).
[20] S. S. Gavrilov, Phys. Rev. B **90**, 205303 (2014).
[21] A. V. Sekretenko, S. S. Gavrilov, and V. D. Kulakovskii, Phys. Rev. B **88**, 195302 (2013).
[22] M. J. Landman, G. C. Papanicolaou, C. Sulem, and P. L. Sulem, Phys. Rev. A **38**, 3837 (1988).
[23] C. Ciuti, P. Schwendimann, and A. Quattropani, Phys. Rev. B **63**, 041303 (2001).
[24] D. M. Whittaker, Phys. Rev. B **63**, 193305 (2001).
[25] S. Gavrilov, A. Brichkin, A. Dorodnyi, S. Tikhodeev, N. Gippius, and V. Kulakovskii, J. Expt. Theor. Phys. Lett. **92**, 171 (2010).
[26] S. S. Gavrilov, A. S. Brichkin, A. A. Demenev, A. A. Dorodnyy, S. I. Novikov, V. D. Kulakovskii, S. G. Tikhodeev, and N. A. Gippius, Phys. Rev. B **85**, 075319 (2012).
[27] J. D. Hunter, Comput. Sci. Eng. **9**, 90 (2007).